POLITECNICO
MILANO 1863

SCUOLA DI INGEGNERIA INDUSTRIALE
E DELL'INFORMAZIONE

Executive Summary of the Thesis

Towards a Multiphysics Modeling Framework for the Human Eye

Laurea Magistrale in Biomedical Engineering - Ingegneria Biomedica

Author: Elisa Bianchini

Advisor: Prof. Rodriguez Matas José Felix

Co-advisor: Prof. Begoña Calvo, Benedetta Fantaci

Academic year: 2025-2026

1. Introduction

The human eye is a part of the sensory nervous system and is the organ responsible for conscious light perception and vision. Its refractive capability and structural integrity depend heavily on the biomechanical properties of its outer layers: the cornea and the sclera. Soft biological tissues like these exhibit non-linear, viscoelastic, and strain-stiffening behaviors. While the cornea features a highly organized, anisotropic network of collagen fibers to ensure optical transparency and mechanical strength, the sclera acts as a robust, predominantly isotropic framework enveloping the posterior globe [1].

Ocular development is a complex and carefully orchestrated process characterized by the precise alignment of tissue growth and optical maturation. A critical metric in this developmental trajectory is the axial length (AL), which represents the axial distance between the apex of the anterior corneal surface and the apex of the posterior scleral surface. It exhibits a bi-exponential growth pattern from embryonic stages through childhood [4], represented in Figure 1.A.

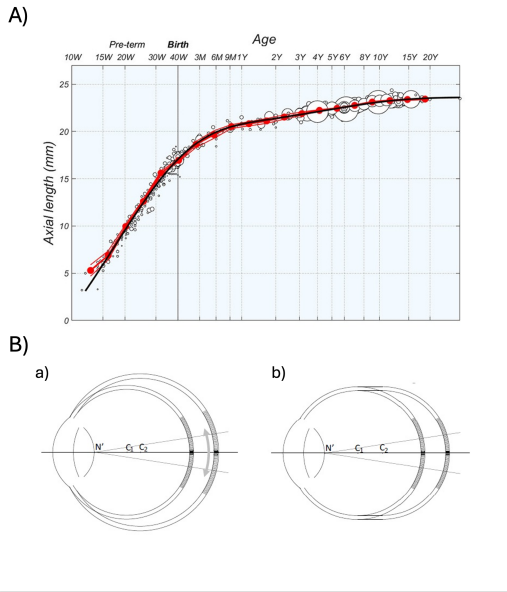

Figure 1: Eye Growth: A) AL as function of age [4]; B) Geometry: a) in the first phase (from the beginning to 1.5 years) and b) in the second phase (from 1.5 years to 20 years).

Specifically, during the initial growth phase, spanning from the gestational period up to 1.5 years of age, the eye expands isotropically in all directions. In the subsequent phase, which lasts until the end of growth, namely up to 20 years of age, corneal growth ceases, and the eye un-

dergoes a predominant axial elongation driven by the sclera [5] (Figure 1.B). This elongation is governed by emmetropization, a homeostatic mechanism that scales the eye's physical dimensions to match its total refractive power, ensuring that incoming light converges precisely on the retina. Morphological imbalances in this growth process, where AL and refractive power fail to align, result in common refractive errors such as myopia and hyperopia.
The main objective of this thesis is to develop a computational framework capable of reproducing the morphological and biomechanical evolution of the human eye from gestation to adulthood. The model aims to:

- Capture the two-stage growth process of the eye
- Incorporate realistic material behavior of ocular tissues
- Analyze the development of internal stresses during growth
- Provide a basis for future multiphysics and clinical models

2. Materials and Methods

The numerical model was developed utilizing COMSOL MULTIPHYSICS, chosen for its versatility in handling complex Partial Differential Equations (PDEs) and its suitability for future multiphysics couplings. The baseline geometry, created from adult eye geometric data found in the literature and comprising the cornea (stroma only), limbus, and sclera, was scaled to represent the 12^{th} week of gestation, targeting an initial AL of 3.279 mm in accordance with experimental data from Rozema et al. [4].

2.1. Material Model

To replicate the behavior of the involved tissues, the *Holzapfel-Gasser-Ogden* (HGO) constitutive model was employed [2]. The parameter values describing the model for each tissue region are summarized in Table 1.
In particular, the strain energy formulation was progressively upgraded:

- **Isotropic Model:** All tissues were modeled using a nearly-incompressible neo-Hookean hyperelastic material model.
- **Anisotropic Model:** The HGO constitutive model was introduced for the cornea and limbus to account for the mechanical contribution of collagen fibers. The biological maturation of these fibers was simulated by linearly decreasing the dispersion parameter κ over time, transitioning the tissue from an isotropic embryological distribution to a fully aligned, mature structural architecture, which is reached at birth (Figure 2.b). Specifically, once fully developed, the cornea features two families of fibers oriented in the superior-inferior and nasal-temporal directions, perpendicular to each other, and a family of limbal fibers oriented circumferentially, as depicted in Figure 2.a.

Tissue	C_{10} **[MPa]**	k_1 **[MPa]**	k_2 **[-]**	K **[MPa]**
Cornea	0.03	0.02	400	5.5
Limbus	0.03	0.02	400	5.5
Sclera	0.70	*N/A*	*N/A*	5.5

Table 1: Material parameters implemented in the Anisotropic HGO Model .

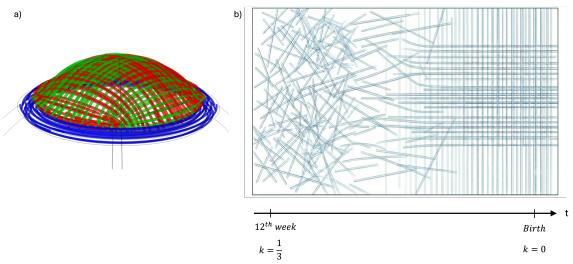

Figure 2: a) Collagen fiber families orientation in the anisotropic model, b) Evolution of the fiber orientation related to the parameter κ.

2.2. Growth formulation

The kinematics of tissue development were simulated using finite growth theory, formulated by Rodriguez et al. [3], within a large-strain continuum mechanics framework.
When a body is subjected to growth or external loads, its motion from an unloaded reference configuration $\mathcal{B}_0$ to a current spatial configuration $\mathcal{B}_t$ is described by the mapping $\mathbf{x} = \boldsymbol{\varphi}(\mathbf{X}, t)$. The fundamental kinematic quantity governing this transformation is the deformation gradient $\mathbf{F} = \nabla\boldsymbol{\varphi} = \partial\mathbf{x}/\partial\mathbf{X}$.
To model biological maturation, this tensor is multiplicatively decomposed into a growth ten-

sor $\mathbf{F}_g$ and an elastic tensor $\mathbf{F}_e$ (Figure 3.a):

$$\mathbf{F} = \mathbf{F}_e \cdot \mathbf{F}_g \tag{1}$$

$\mathbf{F}_g$ acts independently at each material point to define local mass addition, generating an intermediate, stress-free configuration $\widehat{\mathcal{B}}_0$. Because non-uniform local growth can induce physical discontinuities, the elastic component $\mathbf{F}_e$ must intervene. It restores spatial compatibility and ensures the continuity of the body, inevitably generating internal residual stresses in the process. The associated local volume changes are characterized by their respective Jacobians ($J = \det(\mathbf{F}) > 0$, $J_e = \det(\mathbf{F}_e) > 0$, $J_g = \det(\mathbf{F}_g) > 0$), which transform the volume elements across the three configurations:

$$dv = J_e \, d\widehat{V} = J \, dV, \quad d\widehat{V} = J_g \, dV \tag{2}$$

where dV, $d\widehat{V}$, and dv denote the volume elements in $\mathcal{B}_0$, $\widehat{\mathcal{B}}_0$, and $\mathcal{B}_t$, respectively.

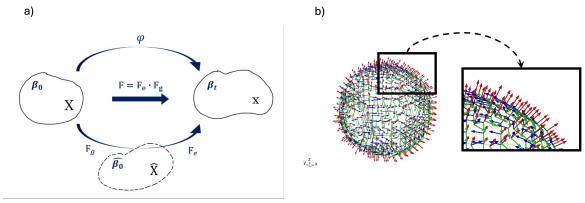

Figure 3: a) Multiplicative split of the deformation gradient, b) Schematic representation of local coordinate system.

To accurately replicate the growth of anatomical structures, $\mathbf{F}_g$ is not defined in a global cartesian framework but rather as a diagonal tensor within a specific local coordinate system (Figure 3.b). This implies a purely unidirectional growth independent along each principal axis, without shear coupling.
The diagonal components of $\mathbf{F}_g$ are governed by a time-dependent volumetric function $\theta(t)$:

$$\mathbf{F}_g = \begin{bmatrix} \theta(t) & 0 & 0 \\ 0 & \theta(t) & 0 \\ 0 & 0 & \theta(t) \end{bmatrix} \tag{3}$$

To implement the developmental hypothesis proposed by Wang et al. [5] within the computational environment, the biological timeline was mapped onto a normalized simulation time interval $t \in [0, 2]$. Specifically, $t = 0$ corresponds to the 12$^{\text{th}}$ week of gestation, $t = 1$ represents the transition point at approximately 1.5 years of age, and $t = 2$ denotes full maturation at 20 years.
The simulation framework divides ocular growth into two distinct morphological phases. This transition from a spatially uniform radial expansion to a highly localized posterior scleral elongation is governed by the continuous, time-dependent volumetric growth function $\theta(t)$ and the spatial gradient function $\text{Mask}_X(\mathbf{X})$:

$$\theta(t) = \begin{cases} 6.625 - 3.15e^{-8.2t} - 2.475e^{-4t} & \text{for } 0 \le t < 1 \\ \theta_1 + 1.7 \cdot \text{Mask}_X(\mathbf{X}) \left(1 - e^{-3(t-1)}\right) & \text{for } t \ge 1 \end{cases} \tag{4}$$

$$\text{Mask}_X(\mathbf{X}) = \max\left(0, \min\left(1, \frac{X - X_{\text{start}}}{X_{\text{end}} - X_{\text{start}}}\right)\right) \tag{5}$$

where $\theta_1 = 6.625 - 3.15e^{-8.2} - 2.475e^{-4}$ acts as a mathematical continuity term evaluated at the end of the first growth phase.

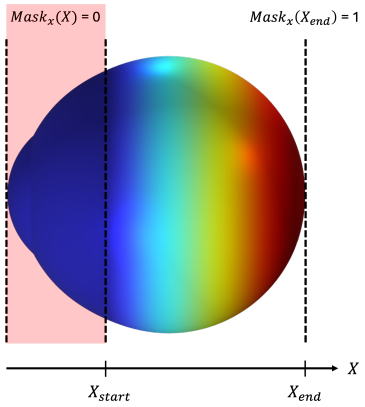

Figure 4: Graphical representation of the application of $\text{Mask}_X(\mathbf{X})$: in the anterior segment of the eye, growth is inhibited, while in the posterior region, it is progressively and linearly applied along the axis.

During the initial phase, the growth rate relies solely on the time-dependent terms. This induces a global radial expansion where all ocular components expand multi-directionally, resembling an inflating balloon.
Conversely, the second phase models the emmetropization process via equatorial longitudinal stretching. The strategic application of the spatial mask, effectively inhibits growth at the anterior segment (Figure 4). This preserves the

corneal dimensions while ensuring a smooth, linear activation of growth towards the internal posterior apex of the sclera, successfully driving the localized axial elongation.

2.3. FE Model

The computational model was implemented within the COMSOL MULTIPHYSICS environment, where the governing mechanical equations were mathematically formulated utilizing the Weak Form Partial Differential Equations (PDEs) interface. To establish a simplified foundational model, the intraocular pressure (IOP) and external boundary loads were omitted. Free, concentric volumetric expansion was achieved by suppressing rigid body translations and rotations through the implementation of Lagrange multipliers over the entire domain.
A predefined mesh, whose main parameters are summarized in Table 2, was selected and validated via a sensitivity analysis to optimize computational efficiency without compromising accuracy (Figure 5).

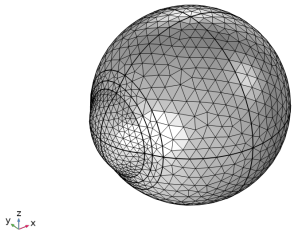

Figure 5: 3D mesh of the eye model.

Mesh Parameter	Value
Max. element size [mm]	0.273
Min. element size [mm]	0.0341
Max. element growth rate	1.45
Curvature factor	0.5
Resolution of narrow regions	0.6

Table 2: Geometric parameters of the predefined mesh implemented in the computational model.

3. Results

3.1. Kinematic Evolution of Ocular Growth

The computational framework successfully reproduced the biphasic macroscopic morphological development of the ocular globe. During the initial isotropic phase (gestation up to approximately 1.5 years of age), the uniform application of the volumetric growth multiplier $\theta(t)$ induced a symmetric, global radial expansion of all structural segments.
Upon entering the emmetropization phase (from 1.5 to 20 years of age), the activation of the spatial gradient function effectively altered the local growth kinematics. As computationally prescribed, the growth magnitude in the anterior segment remained constant at the values reached at the end of the first phase, successfully arresting corneal expansion and preserving its stable dimensions. Concurrently, the posterior sclera underwent a continuous, localized elongation along the anterior-posterior axis. Importantly, the macroscopic kinematic response (nodal displacements) proved identical regardless of the material formulation (isotropic or anisotropic) employed.
The computational geometric trajectories were validated against clinical data. As detailed in Table 3, the simulated AL at the end of both the initial growth phase and the emmetropization process exhibited strong agreement with the experimental targets (Figure 6). Structural thickening also aligned with physiological trends: the central cornea stabilized at 0.476 mm, approximating the physiological average of 0.550 mm, while the sclera progressively thickened to reach a mature dimension of 1.00 mm.

Growth Phase	Experimental Target [mm]	Simulated AL [mm]	Δ [%]
1st phase	21.08	21.41	+1.6
2nd phase	23.65	23.12	-2.2

Table 3: Comparison between physiological targets and computational results for the AL at the end of the two main growth phases.

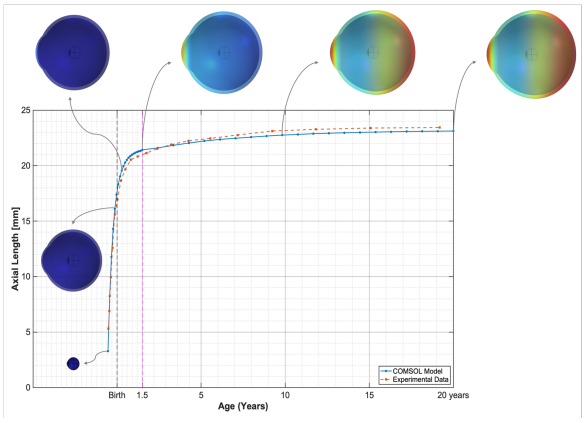

Figure 6: AL values over time, derived from the experimental data by Rozema et al. [4] (orange) and from the computational model (blue). The morphological evolution of ocular growth is also depicted.

3.2. Stress Assessment

The mechanical state of the tissues was evaluated by analyzing the maximum principal stress, which identifies the peak tensile stresses induced by kinematic growth.

During the global expansion phase, the unconstrained, spatially uniform volumetric expansion preserved perfect geometric compatibility. Consequently, neglecting minor numerical approximations, the tissue maintained a globally stress-free state (Figure 7.A). This behavior is consistent with the simplified model assumptions, which intentionally omitted external boundary constraints, as the orbital cavity, and physiological loads, as the IOP.

However, during the second developmental phase, the asymmetric growth profile generated severe kinematic incompatibilities. The differential expansion between the non-growing cornea and the actively elongating posterior sclera forced the tissues to internally accommodate a severe strain discontinuity. This structural mismatch induced the development of a highly localized ring of residual maximum principal stress at the corneoscleral transition boundary (Figure 7.B).

Notably, both the isotropic and anisotropic models captured this transitional stress ring with a highly similar structural response. The peak stress reached approximately 190 Pa in both formulations, with a negligible discrepancy (∼2 Pa). This confirms that, under the current unconstrained conditions, residual stresses are fundamentally driven by the kinematic incompatibilities of the spatial growth gradient, rather than the localized intrinsic anisotropy of the corneal fibers.

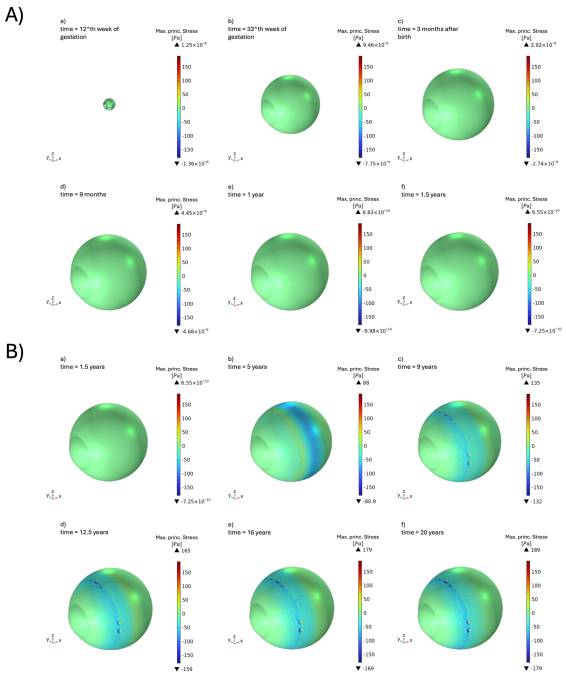

Figure 7: Temporal evolution of the maximum principal stress distribution during A) the first phase and B) the second phase of growth.

4. Discussion

The computational simulations successfully translated the biological growth of the human eye into a continuum mechanics framework, validating the robustness of the model from the gestation phase through adulthood. The numerical model accurately replicated the two distinct developmental phases of the eye: an initial uniform radial expansion representing early fetal and infant development (up to 1.5 years of age), followed by a localized axial elongation of the posterior sclera (up to 20 years of age), which effectively captures the emmetropization process. The predicted morphological parameters, particularly the AL and the corneal and scleral thickness, showed excellent agreement with clinical data. While slight discrepancies in the final AL value were observed, these can be considered negligible given the high dispersion and variance inherent in the original experimental data [4], confirming the predictive validity of the adopted growth multiplier approach.

Furthermore, the analysis of the internal stress

field provided crucial insights into the kinematics of finite growth. During the initial isotropic growth phase, the uniform expansion translated into a fully compatible intermediate configuration, allowing the tissue to expand without developing internal residual stresses ($\mathbf{F}_e \approx \mathbf{I}$). Conversely, the asymmetric growth imposed during the second phase introduced geometric incompatibilities between the static cornea and the elongating sclera. To restore tissue continuity, the system was forced to undergo non-zero elastic deformations, generating residual stresses localized primarily in the transitional regions. Notably, the peak principal stresses were nearly identical in both models, demonstrating that these residual stresses are driven by the kinematic incompatibilities of the spatial growth gradient rather than the intrinsic material anisotropy.
However, these findings must be interpreted in light of the current model's limitations. The computational framework represents a simplified baseline that deliberately neglects the IOP and the biological structures surrounding the eye within the orbital cavity. *In vivo*, these surrounding tissues would impose external physical constraints on the globe, likely modulating the overall stress distribution and the mechanical response of the eye.

5. Conclusion and Future Developments

This thesis successfully established a functional, continuum mechanics-based computational framework capable of tracing the complex biomechanical growth of the human eye. By accurately reproducing the experimental data evolution of the biphasic clinical kinematics and uncovering the mechanical origins of residual transitional stresses, the study provides a robust numerical foundation for ocular biomechanics.
While the current unconstrained model serves as a robust baseline, its simplifications pave the way for sequential multiphysics enhancements. Future developments will prioritize the integration of the IOP, initially as a constant physiological internal load and subsequently through a fully coupled fluid dynamics model to simulate fluid secretion and dynamic IOP evolution.
Further advancements will incorporate the crystalline lens to enable a complete optomechanical coupling, allowing for the comprehensive assessment of visual performance. Additionally, integrating biochemical stimuli into the governing PDEs will facilitate the simulation of pathological growth conditions, such as myopia. Finally, the application of realistic boundary conditions representing the orbital cavity, combined with patient-specific topographic meshes, will transform this framework into an advanced predictive tool for clinical diagnostics and refractive surgery planning.

References

[1] Daniel G. Dawson, Mitchell A. Watsky, Dayle H. Geroski, and Henry F. Edelhauser. *Duane's Ophthalmology*. Lippincott Williams & Wilkins, 2009.

[2] T. Christian Gasser, Ray W. Ogden, and Gerhard A. Holzapfel. Hyperelastic modelling of arterial layers with distributed collagen fibre orientations. *Journal of the Royal Society Interface*, 3:15–35, 2006.

[3] E. Rodriguez, A. Hoger, and A. McCulloch. Stress-dependent finite growth in soft elastic tissues. *Journal of Biomechanics*, pages 455–467, 1994.

[4] Jos J. Rozema. Refractive development I: Biometric changes during emmetropisation. *Ophthalmic and Physiological Optics*, 43(3):347–367, 2023.

[5] Yiyi Wang, Nicolas Bensaid, Pavan Tiruveedhula, Jianqiang Ma, Sowmya Ravikumar, and Austin Roorda. Human foveal cone photoreceptor topography and its dependence on eye length. *eLife*, 8, 2019.